Optimizing Ga-profiles for highly efficient Cu(In, Ga)Se_2 thin film solar cells in simple and complex defect models

OPEN ACCESS
IOP Publishing
Journal of Physics D: Applied Physics
J. Phys. D: Appl. Phys. **47** (2014) 485104 (12pp)
doi:10.1088/0022-3727/47/48/485104

Optimizing Ga-profiles for highly efficient Cu(In, Ga)Se_2 thin film solar cells in simple and complex defect models

C Frisk[1], C Platzer-Björkman[1], J Olsson[1], P Szaniawski[1], J T Wätjen[1], V Fjällström[1], P Salomé[2] and M Edoff[1]

[1] Ångström Solar Center, Division of Solid State Electronics, Uppsala University, Ångström Laboratory, Box 534, SE-751 21, Uppsala, Sweden
[2] International Iberian Nanotechnology Laboratory, Laboratory for Nanostructured Solar Cells, Av. Mestre José Veiga, 4715-330 Braga, Portugal

E-mail: christopher.frisk@angstrom.uu.se

Received 7 July 2014, revised 11 October 2014
Accepted for publication 16 October 2014
Published 13 November 2014

Abstract

Highly efficient Cu(In,Ga)$(S,Se)_2$ photovoltaic thin film solar cells often have a compositional variation of Ga to In in the absorber layer, here described as a Ga-profile. In this work, we have studied the role of Ga-profiles in four different models based on input data from electrical and optical characterizations of an in-house state-of-the-art Cu(In,Ga)Se_2 (CIGS) solar cell with power conversion efficiency above 19%. A simple defect model with mid-gap defects in the absorber layer was compared with models with Ga-dependent defect concentrations and amphoteric defects. In these models, optimized single-graded Ga-profiles have been compared with optimized double-graded Ga-profiles. It was found that the defect concentration for effective Shockley–Read–Hall recombination is low for high efficiency CIGS devices and that the doping concentration of the absorber layer, chosen according to the defect model, is paramount when optimizing Ga-profiles. For optimized single-graded Ga-profiles, the simulated power conversion efficiency (depending on the model) is 20.5–20.8%, and the equivalent double-graded Ga-profiles yield 20.6–21.4%, indicating that the bandgap engineering of the CIGS device structure can lead to improvements in efficiency. Apart from the effects of increased doping in the complex defect models, the results are similar when comparing the complex defect models to the simple defect models.

Keywords: model thin film solar cells, simulations, Ga-profile, optimization

(Some figures may appear in colour only in the online journal)

1. Introduction

Lab-scale chalcopyrite thin film solar cells have had a slow but steady climb in power conversion efficiency in the last decade, marked by the National Renewable Energy Laboratory (NREL) reaching the 20% milestone with a co-evaporated Cu(In,Ga)Se_2 (CIGS) solar cell in 2007 [1]. At the time, it was presented that the record cell had measured efficiency of 19.9%, but later on it was corrected to 20.0% due to a new standard solar spectral irradiance reference. In 2013, ZSW presented several co-evaporated CIGS solar cells above 20% [2] and later a new record cell of 20.8% [3]. In early 2014, Solar Frontier announced a new record at 20.9% for a 0.5 cm^{-2} CIGS solar cell [4], and in June 2014 Solibro presented a CIGS solar cell with 21.0% efficiency [5]; both cells were verified by the Fraunhofer Institute. Swiss Federal Laboratories for Materials Science and Technology (EMPA) holds the current record for CIGS thin film solar cells on

flexible substrates, with 20.4% efficiency [6]. As the efficiency increases towards the ideal Shockley-Queisser limit, it is becoming more difficult to improve it. Much effort has been put into investigation of the absorber layer and its interfaces where the material parameters are critical to the device performance. One of these parameters is the compositional ratio of Ga to In, which is known to influence the conduction band edge energy level [7]. We define this compositional parameter as GGI ≡ Ga/(Ga + In), where we use atomic ratios of respective elements, and the variation of GGI through the depth of the absorber is defined as the Ga-profile. With the ability to control the bandgap throughout the absorber layer, it is possible to introduce quasi-electrical fields, change conduction band alignment, change the absorption regions and suppress recombination pathways.

To study the influence of a GGI-graded absorber one can use modeling, and there are several studies on this topic [8–15]. The conclusions of these studies are diverse, however, where some argue that CIGS absorbers have a double-graded Ga-profile with the highest efficiency of notch yield [8–10, 15]. The primary argument for a notch-type Ga-profile is because of high current density due to absorption in the low bandgap region (notch), while also maintaining high voltage though a larger bandgap in the space charge region (SCR). Other studies are more critical of notch-type GGI-grading, arguing that front grading is detrimental to cell efficiency [11], or that front grading could be detrimental in certain conditions, and that the benefits of any GGI-grading are smaller than commonly believed and dominated by positive effects of the added Ga in itself [12]. Decock *et al* conclude that alternative back grading (flat step in GGI towards the back contact) is redundant for thick absorber layers and that front grading (mainly in the valence band) might be beneficial if it is engineered in such a way that it moves generation to a region with a lower probability of recombination [13]. In general, the consensus is that notch-type GGI-grading is or could be beneficial rather than detrimental, but it is hard to decouple the benefits from grading and the benefits from deposition processes. One example is the three-stage-process, known for yielding high quality CIGS films, where the notch-type Ga-profile is formed as a consequence. Also, one should take care to have a solid framework when comparing different profiles, as pointed out in previous studies [12, 13], and be aware that a varying GGI will also introduce changes in other parameters, e.g. the recombination rate [16]. Moreover, when doing simulations, one needs to be aware that the net effects of GGI-grading are dependent on defect levels and their distributions [13, 15, 17]. Thus, it becomes important to build models on the basis of experimental data in order to be able to predict the effects of changing the Ga-profile. Moreover, the use of data from high quality solar cells is important in order to correctly predict possible enhancements for high efficiency devices.

In this work, we simulated the role of the Ga-profile in the SCAPS software [18] on the basis of experimental data from a reference solar cell. This device is a representative state-of-the-art in-house CIGS solar cell with efficiency $\eta > 19\%$. This reference device was created in a similar fashion to our baseline process [19], with a Mo back contact on top of a soda lime glass, a CIGS absorber layer, a CdS buffer layer, a non-doped ZnO layer (i-ZnO) as well as an Al-doped ZnO layer (ZnO : Al) in connection to the grid fingers. Some small modifications of the baseline process were done to the back and front contacts. The back contact was created by sputtering a thicker Mo layer, with a 15 nm thick evaporated layer of NaF on top, to ensure that enough Na was available during the growth of the CIGS layer. We also used a thinner ZnO and the addition of MgF_2 on top to minimize reflection and parasitic absorption, respectively. The absorber layer deposition for the reference device was done in a batch evaporation tool at 540 °C with a simulated in-line process, see figure 1. This deposition process is similar to our in-line evaporation baseline process [19], but with a small modification towards the end where a front grading is formed. The metal deposition rates shown are the values measured with a quadruple mass spectrometer and corrected with the known composition from x-ray fluorescence (XRF) analysis. In our deposition process, with no temperature gradients during deposition or sharp steps in metal evaporation rates, the Ga-profile is thought to be more decoupled from the absorber film quality as compared to the classical three-stage-process. According to the evaporation data, seen in figure 1, where the integrated CGI ≡ Cu/(Ga+In) and GGI are shown on the right-hand *y*-axis, the CIGS was in slightly Cu-rich state in the first half of the deposition window: CGI peaks at 1.15. The notch is formed 12 min into the deposition process.

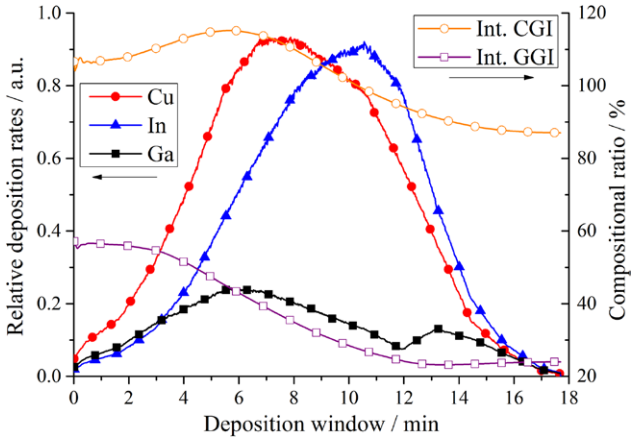

Figure 1. On the left-hand *y*-axis: the evaporation rates as a function of time, measured with a mass spectrometer and corrected with XRF analysis according to the final integrated value of CGI and GGI, which are shown above and related to the right-hand *y*-axis. The sources and substrate are heated prior to the actual deposition window shown above, and subsequently cooled afterwards. The deposition temperature at the substrate holder is 540 °C.

The simulations were done in four different models: two simple defect models with a constant or Ga-dependent absorber defect concentration placed in the middle of the bandgap, and variations of these models with a donor/double acceptor amphoteric defect complex with constant distribution in the CIGS layer. Within these models, single-graded (SG) and double-graded (DG) Ga-profiles were optimized and compared with each other.

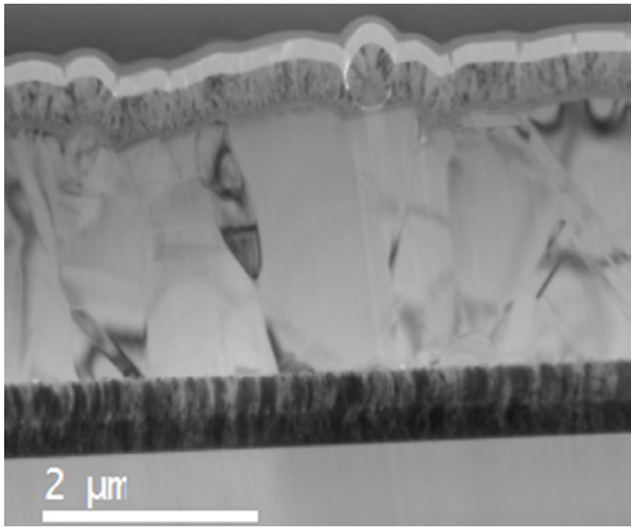

Figure 2. One of the cross-section transmission electron microscopy images of the full stack of the reference device. The different layer thicknesses were estimated and averaged from several spots of the images.

2. Experimental

2.1. Models

Four SCAPS models are described in this study—A, B, C and D—with different defect type and distribution. The models are based upon our earlier baseline model from 2011 [20]. Presented in this work are the most fundamental parameters as well as the new sets of parameters of each model that either have been changed with input from optical or electrical characterization of the actual reference device, or altered to fit with current–voltage (JV) and external quantum efficiency (EQE) measurements of the same device.

Each model consists of a four-layer structure, representing the CIGS, CdS, i-ZnO and ZnO:Al of the reference device. The thickness of each layer is an average of the thicknesses measured with cross-section transmission electron microscopy (TEM), see figure 2.

There are three interfaces considered in the models: the front contact, the interface in between the CIGS and CdS layers, and the back contact. The option to have flat bands in SCAPS was used at both contacts, meaning that the metal work function is dependent on the contacting semiconductor, i.e. the electron affinity, the band edge energies, the density of states and the doping concentration, but no other defects, in order to minimize the metal-semiconductor barrier. At the contacts fixed surface, recombination velocities, S_b and S_f, were set, where S_b was decreased from the previous baseline value 10^7 to $10^6\,\mathrm{cm\,s^{-1}}$ based on a more recent study in the group [21]. In addition, there is an optical filter at the front contact, whereas no reflection is assumed at the back contact. The optical filter corresponds to the reflectance measured with a spectrophotometer with an integrating sphere. This measurement was done on the complete reference solar cell stack. Carrier generation, in each layer, is calculated with wavelength-dependent absorption coefficients [22] and an AM1.5 spectrum. The composition of the CIGS layer was measured with energy dispersive x-ray spectroscopy (EDS) for three individual CIGS grains from our reference device. On each grain we performed and averaged 10 parallel measurements, with a step width of 25 nm. The EDS data were calibrated using the average composition XRF analysis. For this study, the XRF calibration was refined by comparing the absorption edge from EQE of flat Ga-profile CIGS devices with varying Ga content. We used the following empirical expression in the models and for extracting the bandgap from EQE: $E_g = 1.01 + 0.626x - 0.167(x - x^2)$, where x = GGI [23]. In the models an average Ga-profile was used, created from the EDS data of the three individual grains. The shallow acceptor concentration of the CIGS layer was estimated from temperature-dependent capacitance (CV-T) measurements. The reference device was either in a relaxed state, treated at 330 K in darkness for one hour, or in a light-soaked state where it was light-biased with white LED light for one hour at room temperature (RT), and then cooled with constant light bias. A JV-measurement was performed under a halogen lamp with a cold mirror (ELH) and the light intensity was calibrated with the J_{sc} from an EQE measurement [24]. From a dark JV-measurement, the series resistance and the shunt conductance, used as one-diode model parameters in SCAPS, were extracted according to the method presented by Hegedus and Sharfarman [25]. In all models, the recombination centers were placed in the middle of the bandgap in order to act as efficiently as possible; we are not attempting to model the exact and complicated nature of the defect-rich and highly self-compensated CIGS material. Instead, we model an equivalent recombination behaviour to replicate the behaviour of the reference device. The concentration of the recombination centers in the CIGS bulk and the interface trap density at the absorber/buffer interface in each model were set by comparing the simulated four figures of merit, V_{oc}, J_{sc}, FF and η, with their measured counterpart, as well as by comparing the overall shape of the JV-curves. The amphoteric defect concentration was set using CV-T data.

The four different models in this work are described in detail below:

(a) Model A is our simple defect model with bulk and interface mid-gap donor defects, uniformly distributed through the depth of the CIGS layer.
(b) In model B, the bulk defects are set similarly to model A, but with a Ga-dependent concentration in line with previous findings [16]: it is empirically known that for the CIGS, V_{oc} deficit increases with increasing GGI, and classically the best devices have been made with GGI ≤ 0.3 [26]. Two criteria when setting the defect distribution were to set its concentration one order of magnitude higher at GGI = 1 compared to GGI = 0, and the minimum defect concentration at GGI = 0.3.
(c) In model C, the simple defect model is assumed with an additional metastable amphoteric defect complex, treated in previous modeling [18] and set to behave as the Cu and Se di-vacancy (V_{Cu}–V_{Se}) complex [27], with electron/hole capture and emission energies from an experimental investigation [28]. Naturally, with this

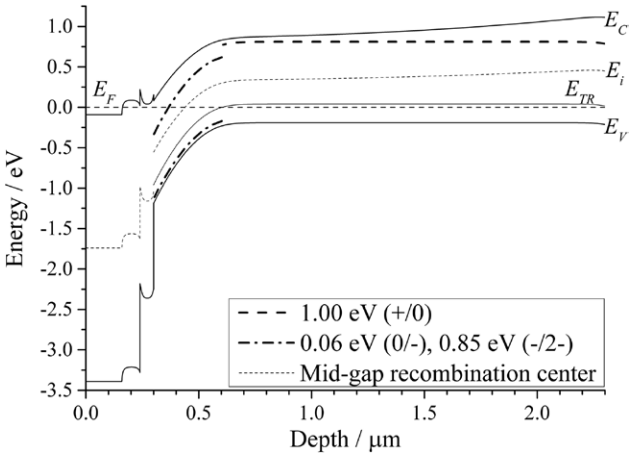

Figure 3. The band diagram of a CIGS device in equilibrium, including (from left to right), ZnO:Al, i-ZnO, CdS and CIGS. The conduction and valence band edge energies are represented as E_C and E_V respectively, and E_i is the intrinsic energy in the middle of the bandgap. In the amphoteric defect model, the position of the Fermi level, E_F, in relation to the amphoteric transition energy, E_{TR}, determines the configuration of the defect complex. In the case shown here, the band bending thus enhances the p-doping of the front region of the CIGS layer, while the back region is compensated.

defect complex there will be an added shallow acceptor and donor concentration, and the p-doping will be either enhanced or partly compensated. As such, the doping of the CIGS is chosen differently [29] than in models A and B. The defect levels of the V_{Cu}–V_{Se} complex can be seen in figure 3.

(d) Model D is a combination of models B and C, including both a Ga-dependent defect distribution and the metastable amphoteric defect complex.

Radiative recombination is taken into account in each model; it was not present in the previous baseline model due to a dominating Shockley–Read–Hall (SRH) recombination. However, it was observed that radiative recombination had an impact for highly efficient CIGS with low bulk defect concentration, especially in the case of notch-type Ga-profiles allowing accumulation of minority carriers at a notch [30].

All individual defects in these models are set with a uniform energy distribution, i.e. single energy level, in the bandgap. The distribution as discussed in this work refers to the depth of the CIGS layer.

2.2. Simulations

Three main sets of simulations were performed in this study: (1) to finalize model A, B, C and D in order to fit them with the reference device data by setting the magnitude of the defect concentrations, (2–3) to see how the efficiency could be improved by changing the CIGS composition and optimizing the Ga-profiles in each model. In detail:

(1) The bulk defect concentration, distinguished by the model, was varied together with the interface trap density in order to fit the measurement of the reference device.

(2) The optimum SG Ga-profile was found by varying the value of GGI at the CIGS/CdS interface and at the back interface of the CIGS layer.

(3) The optimum DG Ga-profile was found with the same steps mentioned in part (2), and by additionally varying GGI at the notch in between the two interfaces, as well as the position of the notch in the CIGS layer.

SCAPS allows the user to create layers with a spatial resolution of 1 nm or manipulate a certain layer with even higher resolution. For simplification in the process of optimizing the Ga-profiles, a spatial resolution in the order of 10 nm was used, and the optimized Ga-profiles were restricted to linear gradients in between points of interest.

3. Results and discussion

3.1. Material characterization

In this section, the results from the material characterization are presented, and a list of model parameters, based on the material characterization, fitting of JV-data and previous studies, can be found in table 1. A TEM image of the reference device from which the layer thicknesses were estimated, can be seen in figure 2. Marked is the average measured CIGS absorber thickness. The window layers are both thinner (310 nm) in our reference device than in the baseline (440 nm), and the Mo back contact is 550 nm in our device instead of 350 nm which is the baseline. The CIGS and CdS thicknesses are similar to those normally used in the group. The EDS data of Ga-profiles for three different grains can be seen in figure 4. The difference in composition at the notch is 5% GGI between grain 1 and grain 3, which corresponds to a bandgap variation of about 25 meV. The thickness of the absorber varies 225 nm between grain 2 and grain 3. Note that the position of the notch from the CIGS/CdS interface is similar for all three grains even if the total thickness varies. The average profile (line in figure 4) was used in order to fit the models with the reference data, but the thickness of this profile was chosen according to the average CIGS thickness from the measurement seen in figure 2, and correlates with the thickness of grain 1. The composition of the reference sample is CGI = 0.87, an average measured with XRF, and GGI = 0.24, calculated for the average EDS profile using the refined XRF data.

The doping concentration of the CIGS layer was estimated from the derivative of the Mott-Schottky plot of the CV-T measurements seen in figure 5. According to Cwil *et al*, the doping concentration is given by the minimum of the net doping concentration curve [29]. In models A and B, this apparent doping concentration corresponds to $N_A \approx 7 \times 10^{15}\text{cm}^{-3}$ for the CV-measurement of the light-soaked reference device at RT. The main reason to choose the doping concentration from this measurement is that the JV-measurement, used to fit the defect concentrations in the model, was performed under prolonged illumination from the ELH lamp in the JV-setup. As such, the RT CV-measurement of the light-soaked reference device is assumed to best fit the models without considering the extra amphoteric defect complex. For reference, the RT

Table 1. The model parameters used for simulations in the SCAPS software. CB DOS and VB DOS stand for conduction band and valence band effective density of states, respectively.

Layer parameter	Symbol (unit)	ZnO : Al	i-ZnO	CdS	CdS/CIGS	CIGS
General						
Thickness	d (nm)	230	80	50	—	1950
Bandgap	E_g (eV)	3.3	3.3	2.4	—	1.0–1.6 (Ga-dep.)
Electron affinity	χ (eV)	4.4	4.4	4.2	—	4.5–3.9 (Ga-dep.)
Rel. permittivity	ε_r	9	9	5.4	—	13.6
CB DOS	N_C (cm^3)	3×10^{18}	3×10^{18}	1.3×10^{18}	—	6.8×10^{17}
VB DOS	N_V (cm^3)	1.7×10^{19}	1.7×10^{19}	9.1×10^{19}	—	1.5×10^{19}
Effective mass	m_h^*, m_e^* (m_e)	0.78, 0.24	0.78, 0.24	0.51, 0.14	0.72, 0.09	0.72, 0.09
Mobility	μ_h, μ_e (cm^{2}V^{-1}s^{-1})	31, 100	31, 100	20, 72	—	13, 100
Doping:						
Type	—	Donor	Donor	Donor	—	Acceptor
Conc.	N_A, N_D (cm^{-3})	10^{20}	10^{17}	5×10^{17}	—	7×10^{15} (A, B), 1.1×10^{16} (C, D)
Radiative rec.	R_B (cm^{3}s^{-1})	10^{-10}	10^{-10}	10^{-10}	10^{-10}	10^{-10}
S. rec. velocity (front, back)	S_f, S_b (cm s^{-1})	10^7 (front)	—	—	—	10^6 (back)
Defects						
Defect I						
Type	—	Acceptor	Acceptor	Acceptor	Donor	Donor
Distribution	—	Constant	Constant	Constant	—	Constant (A, C), Ga-dep. (B, D)
Conc., density	N_T, N_{IF} (cm^{-3}, cm^{-2})	10^{16}	10^{16}	2×10^{17}	10^{12}	Model dep., see figure 7
Energy level	E_T	E_i	E_i	E_i	E_i	E_i
Cap. cross-sec.	σ_p, σ_n (cm^2)	5×10^{-13}, 10^{-15}	5×10^{-13}, 10^{-15}	5×10^{-13}, 10^{-15}	10^{-15}, 5×10^{-13}	10^{-15}, 5×10^{-13}
Defect II						
Type	—	—	—	—	—	Amphoteric (C, D)
Distribution	—	—	—	—	—	Constant
Conc.	N_T (m^{-3})	—	—	—	—	9×10^{15}
Energy level	E_T (eV); above E_V	—	—	—	—	1.00 (+/0) / 0.06, 0.85 (0/-, -/2-)
Cap. cross-sec.	σ_p, σ_n (cm^2)	—	—	—	—	10^{-17}, 10^{-17}

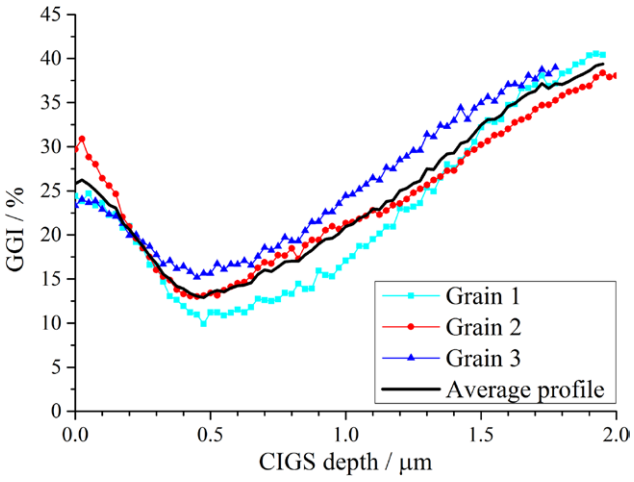

Figure 4. GGI as a function of the depth of the CIGS layer, i.e. the Ga-profiles, for three individual grains of the reference device, measured with energy dispersive x-ray spectroscopy. Each individual Ga-profile is an average from 10 separate line scans performed on each grain, with a step width of 25 nm. In the simulations, we use a calculated average of the three individual Ga-profiles (line).

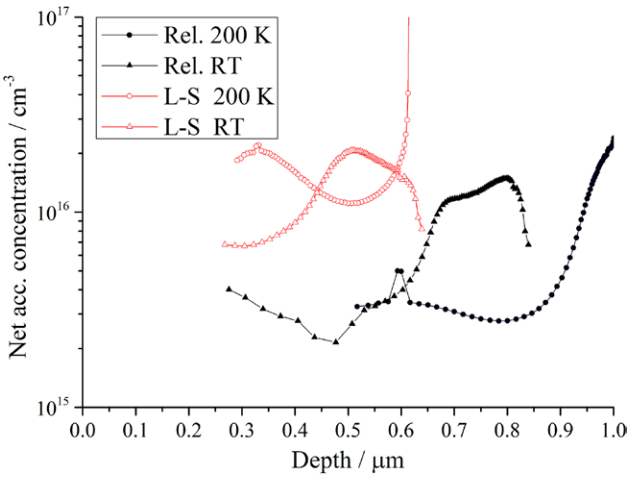

Figure 5. The net acceptor concentration derived from the CV-measurements of the reference device. The relaxed (Rel., black curves) device was kept in darkness at 330 K for one hour and then cooled. The light-soaking (L-S, red curves) was achieved with about 0.1 W cm^{-2} white LED light for one hour at 330 K, and then cooled with constant light bias before the measurement.

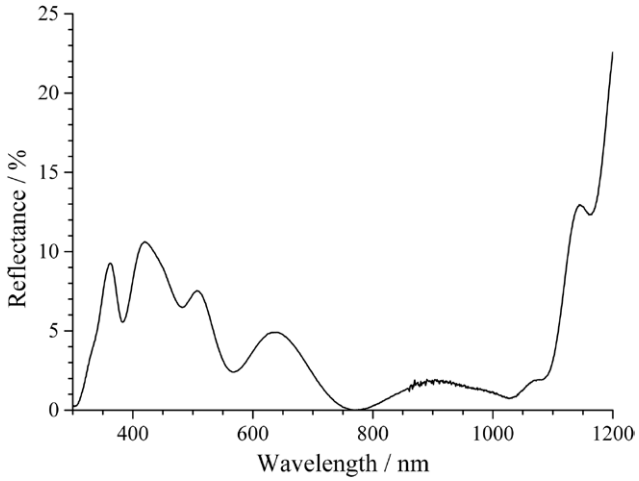

Figure 6. The reflectance of the full stack was measured and is used as an optical filter, as shown above, in the EQE-simulations. For JV-simulations, the whole curve is shifted 2.5% up to compensate for the area of the grid fingers, shadowing the active area of the solar cell.

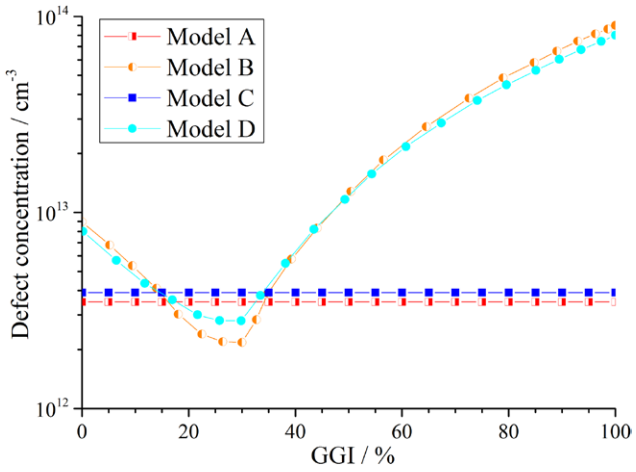

Figure 7. The single level mid-gap donor recombination center concentration as a function GGI in each model. The difference in concentration between models A and C, as well as the similar difference between models B and D, is a consequence of a higher degree of freedom when fitting V_{oc} in models with higher doping concentration (models C and D).

CV-measurement for the relaxed reference device is included in figure 5.

In models C and D, when introducing the V_{Se}–V_{Cu} amphoteric defect complex, we also introduce the availability of more shallow acceptors or compensational shallow donors depending on the configuration of the defect complex. In theory [27], the $V_{Se} - V_{Cu}$ complex in a relaxed solar cell will appear in the acceptor configuration close to the CIGS/CdS interface, where the band bending causes the Fermi level to rise above the amphoteric transition energy (E_{TR} = 0.23 eV in our models), and it will appear in a donor configuration some distance from the CIGS/CdS interface, where the Fermi level is below E_{TR} for a device in equilibrium. The assumption is made that for a low temperature CV-measurement of the relaxed reference device, the minimum of the net acceptor concentration corresponds to maximum compensation, i.e. the V_{Se}–V_{Cu} complex in 100% donor configuration. In contrast, the peak net acceptor concentration, measured from the light-soaked CIGS reference device at low temperature, was assumed to correspond to the V_{Se}–V_{Cu} complex in 100% acceptor configuration. From these assumptions, the doping and amphoteric metastable defect concentrations were derived. The value of the amphoteric defect concentration at $N_T = 9 \times 10^{15}\,cm^{-3}$ in this work corresponds well with the values presented in previous studies [18, 29].

The optical reflectance data from the reference device is seen in figure 6, and the minimum around 770 nm corresponds to negligible reflection. This agrees very well with the chosen MgF_2 thickness at around 140 nm, optimized to fit the peak photon flux of the AM1.5 spectra. The plot shows the reflectance of active area and was used as an optical filter for EQE simulations. For JV-simulations the reflectance was uniformly shifted up 2.5% absolute corresponding to the shadowing area of the front contact grid fingers.

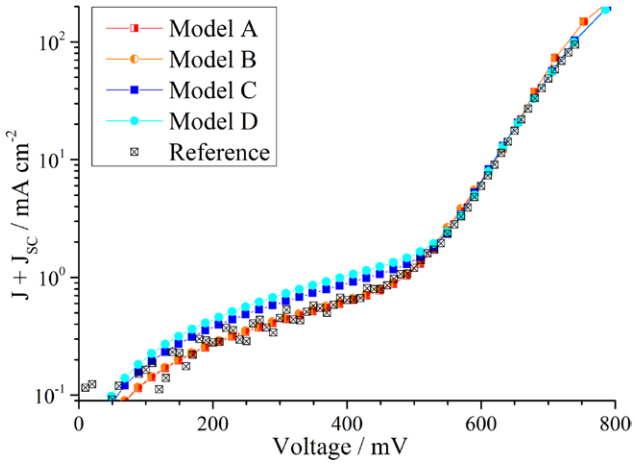

Figure 8. The JV-simulations of all models, A–D, and the measured JV-data of the reference device. As can be seen in the graph, models A and B have better current collection than models C and D, which seems to fit better with the reference device in this region ($V < V_{mp}$). For higher voltages, the diode behavior of models C and D seem to fit better with the reference device.

3.2. Models

The fit between simulations and JV-measurement data from the reference device was made by adjusting the defect concentrations in each model, as seen in figure 7 and table 1. The plots of corresponding JV-simulations and JV-parameters can be seen in figure 8 and table 2, respectively. Noticeable is the low bulk defect concentration that has been used in all models, in the order of $10^{12}\,cm^{-3}$. In reality, CIGS is defect-rich, and this low number represents an effective concentration of recombination centers in the absorber layer that makes the best fit in our models. The recombination rate is exponentially decaying with the increasing difference of the defect energy level in respect to the intrinsic level. In other words, with fixed

Table 2. The simulated JV-parameters for the four models and the measured JV-parameters from the reference device from which many of the input parameters have been taken. Assuming a one-diode model behavior, J_0 and A were extracted by fitting the one-diode model equation to the corresponding JV-data.

Model	V_{oc} (mV)	J_{sc} (mA cm^{-2})	FF (%)	η (%)	J_0 (A cm^{-2})	A
A	680	38.1	75.7	19.6	4.5×10^{-10}	1.45
B	681	38.0	75.4	19.5	6.1×10^{-10}	1.47
C	687	37.8	75.6	19.6	3.7×10^{-10}	1.45
D	685	37.6	75.8	19.5	4.5×10^{-10}	1.46
Reference	685	36.8	75.9	19.1	1.38×10^{-9}	1.56

capture cross-sections, the defect concentration set here is the minimum defect concentration for this recombination rate for a single level defect of this type with uniform distribution through the depth of the absorber. In these models, back contact surface recombination has an impact equivalent to, or higher than, the recombination in the bulk absorber. The cause of this effect is that the low defect concentrations make the electron diffusion length longer, so the influence of the back contact extends further into the CIGS absorber.

The CIGS/buffer layer interface trap density is much debated and in this work was set to a nominal value [20], 10^{12} cm^{-2}. In one simulation study, Song *et al* mention only a 'high recombination interface layer' [9], while others do not include any interface traps due to their negligible influence for positive conduction band offset (CBO) [12] (true for CBO between around 0 and +0.2 eV), or simply do not mention it at all. A sensitivity analysis shows that in our four SCAPS models, with the reference Ga-profile, the JV-parameters do not change substantially for an interface trap density variation spanning from 10^{11} to 10^{13} cm^{-2}. Recently, NREL presented a study based on time-resolved photoluminescence concluding that SRH and surface recombination are insignificant for high-efficiency CIGS solar cells [31]; this is in accordance with the low bulk defect concentrations and insensitivity to CIGS/buffer layer interface trap densities modeled in this work.

Regardless of the low bulk defect concentrations set in our models, V_{oc} in models A and B was in both cases slightly lower than the experimental value of the reference device. The difference of 4 mV is not considered substantial, but it is interesting to note that, even without recombination in the bulk of the CIGS layer and at the CIGS/CdS interface, the V_{oc} does not increase more than an additional 6 mV, indicating that it is limited by the bulk shallow acceptor concentration, i.e. the doping concentration. In models C and D, with higher shallow acceptor concentration assumed, the measured V_{oc} is no longer on the limit set by the doping.

J_{sc} is higher in all models compared to the reference device, and as seen in figure 9 the simulations overestimate the current generated for all wavelengths, except for long wavelengths at the absorption edge. The general difference in EQE is assumed to originate from the dead cell area. Since the reflection was measured on the full stack, however, and the model is restricted to absorption as the only other optical input parameter, some of the difference in EQE at shorter wavelengths could be caused by interference at the buffer/window

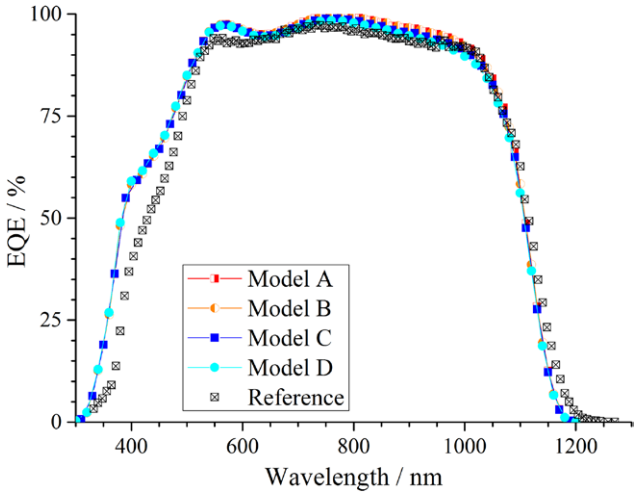

Figure 9. Simulated external quantum efficiency of each model and the measured data from the reference device. A general good fit was achieved by using the reflectance spectrum in figure 6 as an optical filter. The mismatch around 400 nm can be attributed to an incorrect absorption coefficient of CdS and i-ZnO/ZnO:Al, and enhanced parasitic absorption due to internal reflectance which would not be visible in the reflectance of the full stack. The total difference in J_{sc} up to 514 nm is around 0.8 mA cm^{-2}.

layer interface. Also, the difference could partly originate from low absorption coefficients for the CdS and the ZnO in the models. Contribution to the photocurrent in terms of the hole injection from the CdS is small in the models, and is not the cause of the overestimated current in EQE. A quantitative analysis shows that for wavelengths between 300 and 514 nm the overestimated current is 0.84 mA cm^{-2}, about half of the total difference in J_{sc}. A more complex simulation tool with the optical constants of each layer would be required to further analyse this difference. For the reverse relationship at wavelengths longer than about 1100 nm, this could be attributed to reflection at the back contact which is absent in the models. As an effect of J_{sc} being overestimated in the simulations, the efficiency is slightly overestimated as well.

The overall shape of the JV-curve in the forward bias regime $V > V_{mp}$ fits considerably better for models C and D which include amphoteric defects, and where the doping concentration was set higher, as compared to models A and B. In this regime, the diode diffusion current becomes large enough to impact the solar cell performance. The simpler models A and B with lower mid-gap defect concentrations fit better for $V < V_{mp}$, where it is clear that the current collection loss is smaller than for models C and D. Shunt conductance and series resistance were set to equal values in all four models.

3.3. Optimization of single-graded Ga-profiles

The optimum SG Ga-profiles were found by simulating different values for GGI at the back contact and at the CIGS/CdS interface, and the results can be seen in figure 10. The optimized SG Ga-profiles are similar to each other, and compared to the EDS-measured Ga-profile the efficiency is increased by 0.9–1.3%. The JV-parameters are found in table 3, where

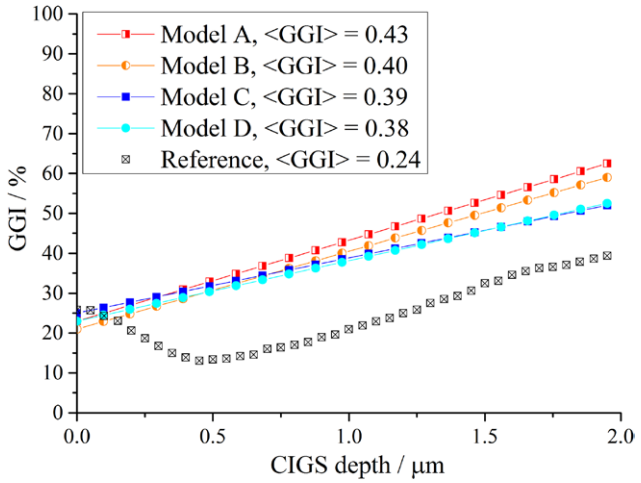

Figure 10. The optimum single-graded Ga-profile, where the distance starts at the front interface. When compared between the models, the results are similar to each other, and the narrow spread at the front interface corresponds to 4% GGI (comparing models B and C). At the back contact the difference is about 10% GGI (between models A and C).

Table 3. The JV-parameters of the optimized single-graded Ga-profiles.

Model	V_{oc} (mV)	J_{sc} (mA cm^{-2})	FF (%)	η (%)	J_0 (A cm^{-2})	A
A-SG	757	34.5	78.9	20.6	7.9×10^{-11}	1.48
B-SG	746	35.1	79.4	20.8	2.8×10^{-11}	1.39
C-SG	747	34.6	79.3	20.5	2.6×10^{-11}	1.38
D-SG	739	35.0	79.7	20.6	0.7×10^{-11}	1.29
Reference	685	36.8	75.9	19.1	1.38×10^{-9}	1.56

the highest efficiency for an optimized SG Ga-profile was achieved in model B, at 20.8%. The overall Ga concentration is higher for these profiles compared to the measured Ga-profile in the reference device, indicating that the efficiency could be improved by increasing GGI in the CIGS layer according to these results, provided that the absorber film quality is unaffected by the compositional variation.

By comparing the Ga-dependent/constant defect concentration models, models B/A, and D/C, it is observed that the models with a Ga-dependent defect distribution have, in general, a lower optimum bandgap value than their counterparts. This difference can be explained by the increase in defect concentration for higher GGI and by the fact that the lowest defect concentration at GGI = 0.3 is lower than the compared constant defect concentration in models A and B. The latter fact means that the total defect concentration of a profile in models B and D is allowed to be smaller than in models A and C, leading to an increase of efficiency for model B compared to A, and model D compared to C. No quantification of the profile differences has been done due to the nature of the selection of the Ga-dependent defect distribution. Experimental verification would be required for cells made with our process, and while the Ga-profile trend is clear, especially for the A/B comparison, the differences are not substantial.

By comparing the models with/without amphoteric defects, models C/A and D/B respectively, we see that

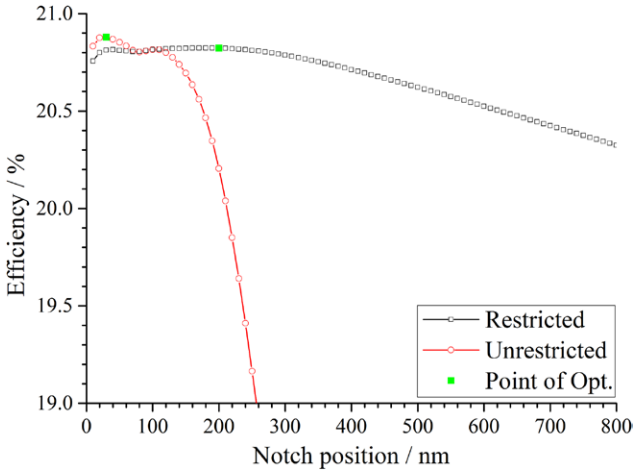

Figure 11. The efficiency as a function of the position of the notch from the CIGS/buffer layer interface. In the unrestricted case, the maximum efficiency was achieved by having the notch 30 nm from the front interface with a very high front grading; however, when placing the notch at 200 nm from the front interface and optimizing the Ga-profile at this point, the efficiency is not lowered more than 0.1%. Moreover, the lower Ga-grading in such a profile lessens the detrimental effects of having the notch further into the bulk.

optimum GGI towards the back contact is lower for the models with amphoteric defects compared to their counterparts, while optimum GGI at the CIGS/CdS interface is slightly higher. This difference is an effect predominantly caused by the increased doping in the models with amphoteric defects; a tradeoff between J_{sc} and V_{oc}, with a small net efficiency gain, makes it more beneficial with a lower GGI towards the back contact for models C and D as compared to models A and B, where optimum GGI is higher towards the back contact. The increase towards the CIGS/CdS interface is partly a net benefit of efficiency due to the tradeoff between V_{oc} and J_{sc}, and partly due to the mitigation of recombination in the SCR via the deep acceptor state of the amphoteric defect complex. The increase in FF originates from the reduced SCR, lowering the recombination that otherwise causes the FF to drop.

In a comparison between respective optimized Ga-profiles, the efficiency is still lower in models C/D, mainly due to a lower $V_{oc,}$ caused by higher recombination in the bulk due to a higher mid-gap defect concentration, compared to models A/B. Moreover, there is additional recombination in models C/D via the deep acceptors at 0.85 eV above the valence band, which is especially effective in the SCR close to the interface.

3.4. Optimization of double-graded Ga-profiles

For optimization of the DG Ga-profiles, it is observed that the position of the notch can play a crucial role depending on the other parameters in the model, e.g. the value of GGI towards the CIGS/CdS interface. In the case of steep front grading, a notch situated in the SCR can suppress detrimental effects, also noted by Gloeckler and Sites [12]. However, in cases of lower front Ga-grading, it is not detrimental to cell performance to have the notch further away from the CIGS/CdS interface. These situations are illustrated in figure 11.

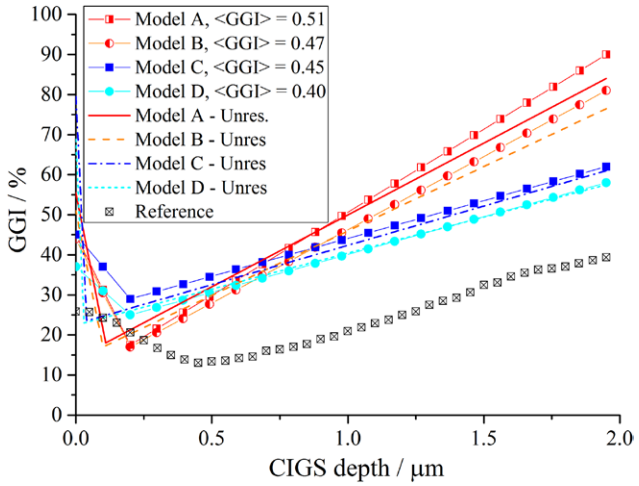

Figure 12. The optimum double-graded Ga-profiles, where the front interface is placed at 0 µm. With the exception of model D, the GGI value at the front interface for the other three models is indistinguishable. The GGI at the notch and back contacts varies mostly due to doping, as seen comparing models A/B with C/D. The Ga-dependent defect models, models B and D, have a slightly lower GGI than their counterparts A and C, respectively.

A maximum efficiency is observed for a notch situated around 80 nm from the CIGS/CdS interface in models A and B, while for models C and D the maximum was observed for a notch situated 30–40 nm into the CIGS layer. In addition, the optimum GGI towards the CIGS/CdS interface, in the cases of models C and D, are 0.8 and 0.7 respectively. These changes of GGI over such short distances are problematic in terms of stability of the CIGS film, and in practice are impossible to realize. Limited control of the CIGS deposition processes, in part due to thermal diffusion, and inter-diffusion that might take place on a larger time scale are the main factors. Therefore, the constraint not to have the notch closer than 200 nm from the CIGS/CdS interface was introduced for the DG Ga-profile optimization process. Figure 11 shows two cases of the extent of the efficiency variation, compared to an optimized point (highlighted), as a function of the notch position in the absorber. The two illustrated cases consider the constrained case where the Ga-profile is optimized for a notch 200 nm from the CIGS/CdS interface, and the unconstrained case where the position of the notch is 30 nm from the CIGS/CdS interface. The two examples mentioned here come from simulations performed in model D, but the constraint on the optimized DG Ga-profile is applied to all four models, see figure 12. Noteworthy is the insensitivity to the notch position observed for the constrained case as seen in figure 11, and more importantly that it exhibits high efficiencies over a wide range of notch positions. In the unconstrained case, the efficiency drops rapidly when the notch is moved further than 100 nm from the CIGS/CdS interface, and this drop is attributed to a rapid drop of FF.

The JV-parameters for the optimized DG Ga-profiles in the four models can be found in table 4 where the parentheses mark the values from the unconstrained process. The highest efficiency of 21.4% is achieved in model B, and 21.2% is achieved in model A. These are the models without amphoteric defects, and the difference is a tradeoff between V_{oc} and J_{sc}, where the simulation in model B has a higher FF due to the lower front grading. When comparing these simulations with the optimum DG Ga-profiles of models C and D, in the former models we see a higher back grading, lower GGI at the notch and therefore a steeper front grading. The difference in back grading is attributed to the difference in doping between the models, similar to the case of optimized SG profiles. The lower and more pronounced notch of models A and B can be attributed to the more extended SCR of these models, due to the lower doping concentration. The simulations show that models C and D, contrary to models A and B, suffer higher SRH recombination via the deep acceptors in the SCR at forward bias due to an increase of minority carriers injected from the buffer layer. Models C and D are in general dominated by SRH recombination throughout the absorber layer. On the other hand, models A and B suffer a dominating radiative recombination current at the notch, which constitutes the critical recombination path due to a high concentration of minority carriers accumulated at the notch. The higher bandgap gradient towards the back contact provides a higher quasi-electrical field, increasing the effective electron diffusion length towards the notch.

3.5. General discussion

The optimized Ga-profiles and the corresponding JV-parameters vary between each model. This shows that there is a dependence on defect-related properties, such as recombination rates and doping concentrations, when optimizing the Ga-profile. Furthermore, it means that a more rigorous electrical analysis is required to have a better understanding and correctly predict the optimum Ga-grading that results in the highest efficiencies for real CIGS thin film solar cells.

Overall, there is a higher efficiency increase in models A and B, when comparing the optimized DG profiles with optimized SG profiles, as compared to models C and D. It increases as much as 0.6% in models A and B, but only 0.1 – 0.2% in models C and D. Nonetheless, the trend is clear: the optimum DG Ga-profiles perform better in simulations than SG profiles within these models, even if the benefit of the DG Ga-profile is marginal. It turns out that interface traps as set in these models play an important role for simulations with SG Ga-profiles. The interface trap density in the four models was set when simulating the measured Ga-profile; however, the power conversion efficiency only changed +0.1% between the case of nominal (10^{12} cm^{-2}) and negligible ($<10^{11}$ cm^{-2}) interface trap densities. In the case of optimized Ga-profiles, the same variation—from the nominal value to negligible amounts of interface trap densities—caused the efficiency of the optimized DG Ga-profiles to have a maximum change of +0.2%, while the optimized SG Ga-profiles had an efficiency change of up to +1.0%. Table 5 summarizes these simulations, and in figure 13 there is a comparison of how the efficiency in model A, with the measured Ga-profile (figure 13(*a*)) and the optimized SG Ga-profile (figure 13(*b*)), varies with bulk

Table 4. The JV-parameters of the optimized DGGa-profiles. The parentheses mark the cases where the DG Ga-profiles were optimized without constraint, i.e. with the notch placed very close to the CIGS/CdS interface.

Model	V_{oc} (mV)	J_{sc} (mA cm^{-2})	FF (%)	η (%)	J_0 (A cm^{-2})	A
A-DG	797 (802)	34.6 (34.4)	77.0 (77.1)	21.2 (21.3)	1.5×10^{-10} (2.3×10^{-10})	1.61 (1.66)
B-DG	790 (790)	35.0 (35.0)	77.4 (77.6)	21.4 (21.5)	0.8×10^{-10} (2.8×10^{-10})	1.55 (1.65)
C-DG	795 (781)	33.5 (34.5)	77.3 (77.0)	20.6 (20.7)	1.1×10^{-10} (4.3×10^{-10})	1.58 (1.67)
D-DG	767 (767)	34.6 (34.8)	78.5 (78.3)	20.8 (20.9)	0.6×10^{-10} (3.4×10^{-10})	1.47 (1.43)
Reference	685	36.8	75.9	19.1	1.38×10^{-9}	1.56

Table 5. The JV-parameters of the optimized single-graded and double-graded Ga-profiles with negligible interface recombination.

Model	V_{oc} (mV)	J_{sc} (mA cm^{-2})	FF (%)	η (%)	J_0 (A cm^{-2})	A
A-SG	797	34.6	76.6	21.1	9.5×10^{-10}	1.78
B-SG	779	35.2	77.7	21.3	4.1×10^{-10}	1.66
C-SG	765	34.7	78.2	20.7	0.5×10^{-10}	1.46
D-SG	759	35.0	78.7	20.9	1.0×10^{-10}	1.50
A-DG	800	34.6	77.0	21.3	2.5×10^{-10}	1.67
B-DG	792	35.0	77.3	21.5	3.0×10^{-10}	1.66
C-DG	800	33.5	77.0	20.7	4.7×10^{-10}	1.72
D-DG	773	34.6	78.2	20.9	0.4×10^{-10}	1.46
Reference	685	36.8	75.9	19.1	1.38×10^{-9}	1.56

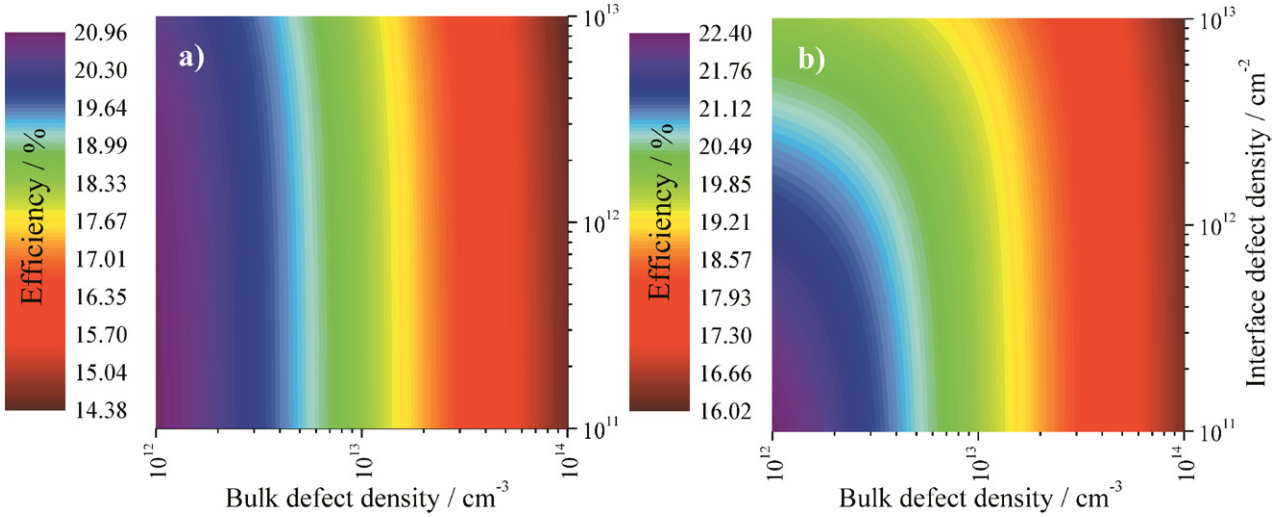

Figure 13. The efficiency as a function of bulk defect concentration and interface trap density in the case of (*a*) the simple defect model A with the measured Ga-profile and (*b*) model A with the optimum single-graded Ga-profile. Clear from figure (*a*) is the insensitivity of interface defects as compared to figure (*b*), which is problematic since the model is set in the conditions corresponding to figure (*a*).

defect concentration and interface trap densities. Due to the nature of these simulations, with the Ga-profile being optimized in only one case (figure 13(*b*), although not for every point), one cannot compare the absolute values of efficiencies between the two plots. Even so, the trend tells us that if the interface traps can be minimized, the DG Ga-profiles might be redundant. Similar findings were found by Hirai *et al* [15].

There are several indications that a more advanced simulation tool would be required in order to achieve a better understanding of the complex behaviour exhibited by our device, such as lateral bandgap fluctuations, electromagnetic interference, interfacial parameter-dependence on the underlying bulk material, metastable transitions, and so on. All of these would be of importance to better understand CIGS. The results from the simulations in all the models point towards the same thing: if the quality of our CIGS can be maintained, compared to the measured Ga-profile of the reference device, we would benefit from increasing the overall GGI in the Ga-profile.

4. Conclusion

In this work, four SCAPS models were studied and compared with experimental data. The models were different in defect concentration and doping values of the CIGS layer: (A) a simple defect model with a constant concentration of mid-gap recombination centers, (B) a model with a Ga-dependent defect concentration, (C) a model with high doping due to

the addition of amphoteric defects, and (D) a combination of models B and C. These models were set to fit a high efficiency reference device with a power conversion efficiency of 19.1%. The device was made with a single stage co-evaporation process and characterized with electrical and optical methods, providing input data for the models. Models A and B exhibited better fit with the reference device measurement for JV-simulation at $V < V_{mp}$, while models C and D exhibited better fit for $V > V_{mp}$. Good fits were achieved with all four models by setting a mid-gap defect concentration in the order of 10^{12}cm^{-3} in the CIGS layer. Simulations with this low defect concentration indicate that bulk SRH recombination is not the dominant limiting factor for our high efficiency CIGS reference device, and one should also consider that, for long minority carrier diffusion lengths, the back contact surface recombination plays a larger part than for more defective CIGS devices.

In each model, single- and DG Ga-profiles were optimized and compared by using JV-simulations. The optimum DG Ga-profiles yielded 0.2–0.6% higher power conversion efficiencies than the SG counterpart in each model. While the original models were insensitive to the interface trap density between the CIGS absorber layer and the CdS buffer layer, it was clear that for the optimized SG Ga-profile the interface trap density plays a role. Back contact surface recombination impacts the choice of optimum Ga-profile as well, and if the back contact could be passivated, the back grading would be less important. Moreover, if the CIGS/buffer layer interface could be passivated, the front grading would become useless, meaning that a SG Ga-profile might be as effective as a DG Ga-profile.

With the effects of different doping concentrations between the complex and simple defect models in mind, the results are consistent. It is obvious that there is potential to change the Ga-profile in the CIGS layer, and thereby enhance the efficiency of solar cells with a simulated in-line deposition process. If the quality of the CIGS absorber layer can be maintained for this deposition process, power conversion efficiency of 21% or above can be achieved by increasing the GGI and deposit Ga-profiles as proposed in this work.

Acknowledgments

The authors gratefully acknowledge the support from Mark Burgelman, previously professor at ELIS University of Gent, who supplied a reference SCAPS definition file, Dr Hiroki Sugimoto from Solar Frontier for an enlightening discussion, Dr Annica Nilsson and Professor Arne Roos at the Solid State Physics department at the Ångström Laboratory for optical measurements, and finally the Swedish Energy Agency, Swedish Research Council and Wallenberg Academy Fellows program for funding.

References

[1] Repins I, Contreras M A, Egaas B, DeHart C, Scharf J, Perkins C L, To B and Noufi R 2008 19.9%-efficient ZnO/CdS/CuInGaSe$_2$ solar cell with 81.2% fill factor *Prog. Photovolt., Res. Appl.* **16** 235–9

[2] Powalla M, Jackson P, Witte W, Hariskos D, Paetel S, Tschamber C and Wischmann W 2013 High-efficiency Cu(In,Ga)Se$_2$ cells and modules *Solar Energy Mater. Solar Cells* **119** 51–8

[3] ZSW 2013 *Press Release 18* (Stuttgart)

[4] Solar Frontier 2014 *Edelman* (Tokyo)

[5] Solibro 2014 CIGS module manufacturing with high deposition rates and efficiencies *40th IEEE Photovoltaic Specialist Conf.* (*Denver, CO, 8–13 June 2014*)

[6] Chirilă A *et al* 2011 Highly efficient Cu(In,Ga)Se$_2$ solar cells grown on flexible polymer films *Nature Mater.* **10** 857–61

[7] Wei S-H, Zhang S B and Zunger A 1998 Effects of Ga addition to CuInSe$_2$ on its electronic, structural, and defect properties *Appl. Phys. Lett.* **72** 3199

[8] Dullweber T, Hanna G, Shams-Kolahi W, Schwartzlander A, Contreras M A, Noufi R and Schock H W 2000 Study of the effect of gallium grading in Cu(In,Ga)Se$_2$ *Thin Solid Films* **361–362** 478–81

[9] Song J, Li S S, Huang C H, Crisalle O D and Anderson T J 2004 Device modeling and simulation of the performance of Cu(In$_{1-x}$,Ga$_x$)Se$_2$ solar cells *Solid State Electron.* **48** 73–9

[10] Huang C-H 2008 Effects of Ga content on Cu(In,Ga)Se$_2$ solar cells studied by numerical modeling *J. Phys. Chem. Solids* **69** 330–4

[11] Topič M, Smole F and Furlan J 1996 Band-gap engineering in CdS/Cu(In,Ga)Se$_2$ solar cells *J. Appl. Phys.* **79** 8537

[12] Gloeckler M and Sites J R 2005 Band-gap grading in Cu(In,Ga)Se$_2$ solar cells *J. Phys. Chem. Solids* **66** 1891–4

[13] Decock K, Lauwaert J and Burgelman M 2010 Characterization of graded CIGS solar cells *Energy Proc.* **2** 49–54

[14] Witte W *et al* 2014 Gallium gradients in Cu(In,Ga)Se$_2$ thin-film solar cells *Prog. Photovolt., Res. Appl.* in press doi:10.1002/pip.2485

[15] Hirai Y, Kurokawa Y and Yamada A 2014 Numerical study of Cu(In,Ga)Se$_2$ solar cell performance toward 23% conversion efficiency *Japan. J. Appl. Phys.* **53** 012301

[16] Hanna G, Jasenek A, Rau U and Schock H W 2001 Influence of the Ga-content on the bulk defect densities of Cu(In,Ga)Se$_2$ *Thin Solid Films* **387** 71–3

[17] Frisk C, Platzer-Björkman C, Fjällström V, Salomé P M P, Olsson J and Edoff M 2013 Modeling Ga-profiles for Cu(In,Ga)Se$_2$ thin film solar cells with varying defect density *Proc. 23rd Int. PVSEC* (*Taipei, Taiwan*) No. 1192

[18] Burgelman M, Decock K, Khelifi S and Abass A 2013 Advanced electrical simulation of thin film solar cells *Thin Solid Films* **535** 296–301

[19] Lindahl J, Zimmermann U, Szaniawski P, Törndahl T, Hultqvist A, Salomé P, Platzer-Björkman C and Edoff M 2013 Inline Cu(In,Ga)Se$_2$ Co-evaporation for high-efficiency solar cells and modules *IEEE J. Photovolt.* **3** 1100–5

[20] Pettersson J, Platzer-Björkman C, Zimmermann U and Edoff M 2011 Baseline model of graded-absorber Cu(In,Ga)Se$_2$ solar cells applied to cells with Zn$_{1-x}$Mg$_x$O buffer layers *Thin Solid Films* **519** 7476–80

[21] Vermang B, Fjällström V, Pettersson J, Salomé P and Edoff M 2013 Development of rear surface passivated Cu(In,Ga)Se$_2$ thin film solar cells with nano-sized local rear point contacts *Solar Energy Mater. Solar Cells* **117** 505–11

[22] Orgassa K 2004 Coherent optical analysis of ZnO/CdS/Cu(In,Ga)Se$_2$ thin film solar cell *PhD Thesis* Der Universität Stuttgart Aachen, Germany

[23] Alonso M I, Garriga M, Durante Rincón C A, Hernández E and León M 2002 Optical functions of chalcopyrite CuGa$_x$In$_{1-x}$Se$_2$ alloys *Appl. Phys.* A **74** 659–64

[24] Hultqvist A, Salome P M P, Fjallstrom V, Edoff M, Aitken B, Zhang K, Shi Y, Fuller K and Williams C K 2013 Performance of Cu(In,Ga)Se_2 solar cells using nominally alkali free glass substrates with varying coefficient of thermal expansion *J. Appl. Phys.* **114** 094501
[25] Hegedus S S and Shafarman W N 2004 Thin-film solar cells: device measurements and analysis *Prog. Photovolt. Res. Appl.* **12** 155–76
[26] Shafarman W N and Stolt L 2003 *Handbook of Photovoltaic Science and Engineering* (New York: John Wiley) p 567
[27] Lany S and Zunger A 2006 Light- and bias-induced metastabilities in Cu(In,Ga)Se_2 based solar cells caused by the (V_{Se}–V_{Cu}) vacancy complex *J. Appl. Phys.* **100** 113725
[28] Urbaniak A and Igalson M 2009 Creation and relaxation of light- and bias-induced metastabilities in Cu(In,Ga)Se_2 *J. Appl. Phys.* **106** 063720
[29] Cwil M, Igalson M, Zabierowski P and Siebentritt S 2008 Charge and doping distributions by capacitance profiling in Cu(In,Ga)Se_2 solar cells *J. Appl. Phys.* **103** 063701
[30] Sugimoto H 2013 Personal communication
[31] Kuciauskas D, Li J V, Contreras M A, Pankow J, Dippo P, Young M, Mansfield L M, Noufi R and Levi D 2013 Charge carrier dynamics and recombination in graded band gap $CuIn_{1-x}Ga_xSe_2$ polycrystalline thin-film photovoltaic solar cell absorbers *J. Appl. Phys.* **114** 154505